Quantifying the Mangrove Cooling Effects on Urban Heat: A Two-Decade Remote Sensing Analysis of Jakarta's Coastal Zone

Andik Isdianto
Department of Marine Sciences, Brawijaya University, Indonesia
andik.isdianto@ub.ac.id (corresponding author)

Intan Astritya Anggraini
Master's Program of Environmental Management and Development, Brawijaya University, Indonesia
intanastritya@student.ub.ac.id

Received: 15 August 2025 | Revised: 13 September 2025 | Accepted: 6 October 2025

 DOI: https://doi.org/10.48084/etasr.14093

ABSTRACT

Urban coastal planning in North Jakarta's Muara Angke–Kapuk requires clear evidence of how land-cover composition influences Land Surface Temperature (LST). This study maps two decades of land-cover change using Object-Based Image Analysis (OBIA), derives LST from Landsat, and applies multiple linear regression across 242 uniform grids (150×150 m) to quantify the LST responses to the built-up area, mangroves, water, ponds, open land, and non-mangrove vegetation. The built-up area expanded from 716.1 to 1,525.1 ha, mangroves increased by 76.7% (183.7ha-324.6 ha), and mean LST increased by 7.5 °C (20.2°C-27.7 °C). The regression achieved a high fit (R^2 = 0.951), with warming associations for the built-up area (B = 1.619 °C), open land (B = 1.139 °C), and cooling associations for mangroves (B = −0.960 °C), water bodies (B = −0.478 °C), ponds (B = −0.275 °C), and non-mangrove vegetation (B = −0.469 °C). These findings indicate that integrating mangrove conservation/restoration with broader green–blue planning can help moderate surface heat along Jakarta's coastal fringe. The OBIA–Landsat workflow provides a transferable, cost-effective basis for routine monitoring and supports climate-resilient urban development by linking land-cover management to LST mitigation in data-limited tropical megacities.

Keywords-urban heat island; land surface temperature; OBIA; mangrove cooling effect; Jakarta Bay

I. INTRODUCTION

Mangrove forests underpin key coastal services—shoreline protection, carbon sequestration, habitat, water purification, fisheries, and ecotourism [1]—yet have declined substantially due to urban expansion, land conversion, aquaculture, and climate pressures [2], weakening coastal resilience and blue-carbon capacity [1, 2]. Remote sensing and GIS offer consistent, multi-scale monitoring of the mangrove extent and condition [3]. In coastal North Jakarta (Jakarta Bay), the fast reclamation and infrastructure development have transformed land use, replacing natural cover with impervious surfaces and intensifying the urban heat island effects, evident in rising land-surface temperatures [4, 5]. North Jakarta exemplifies these dynamics, with research reporting measurable temperature increases [6].

Despite the numerous global assessments of mangrove loss and urbanization, integrated, site-specific analyses that link long-term land-cover trajectories with LST in urban mangrove systems remain limited. Addressing this gap, the current study provides a joint assessment for the Muara Angke Kapuk (MAK) mangrove system across 2005, 2010, 2015, 2020, and 2024, coupling high-resolution object-based land-cover mapping with Landsat-derived LST.

The contributions of this study are: (i) a harmonized, multi-epoch land-cover dataset for a rapidly urbanizing coastal fringe, (ii) a spatiotemporal characterization of LST change, and (iii) a quantitative assessment of the relationships between land-cover composition and LST. The results inform climate-resilient coastal planning by documenting the moderating role of mangroves and other green-blue covers on surface heat in a tropical megacity context.

II. MATERIALS AND METHODS

A. Satellite Data Sources and Processing Workflow

Analyses were conducted at five epochs (2005, 2010, 2015, 2020, 2024). Land cover was delineated from Google Earth Pro mosaics (approximately 2 m) using OBIA. LST was retrieved from Landsat-7 ETM+ Band 6 (2005, 2010; 60 m resampled to 30 m, SLC-off gaps gap-filled) and Landsat-8 TIRS Band 10 (2015, 2020, 2024; 100 m resampled to 30 m), with emissivity derived from OLI-based NDVI. The satellite data sources used in this study are presented in Table I. All imagery underwent

geometric/radiometric pre-processing; OBIA in eCognition and spatial analyses in ArcGIS/QGIS. The Workflow for land-cover mapping and LST retrieval is shown in Figure 1.

B. Study Area

The study area spans the coastal fringe of Penjaringan, North Jakarta, including newly reclaimed islands, built-up areas, water bodies, aquaculture ponds, open land, and the approximately 4,248.6 ha Muara Angke–Kapuk mangroves. Rapid urban growth and reclamation since the 1990s make it a representative urban–ecological interface of Southeast Asian megacities. Satellite images from 2005, 2010, 2015, 2020, and 2024 were analyzed to assess the land-cover change and land-surface temperature before and after reclamation, as depicted in Figure 2.

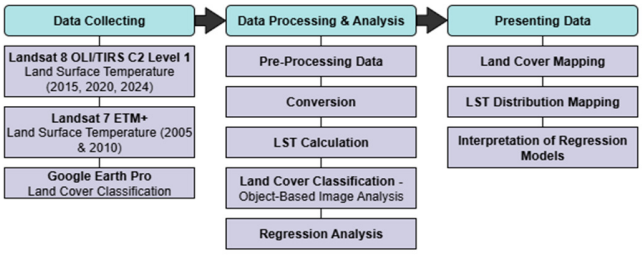

Fig. 1. Workflow for land-cover mapping and LST retrieval.

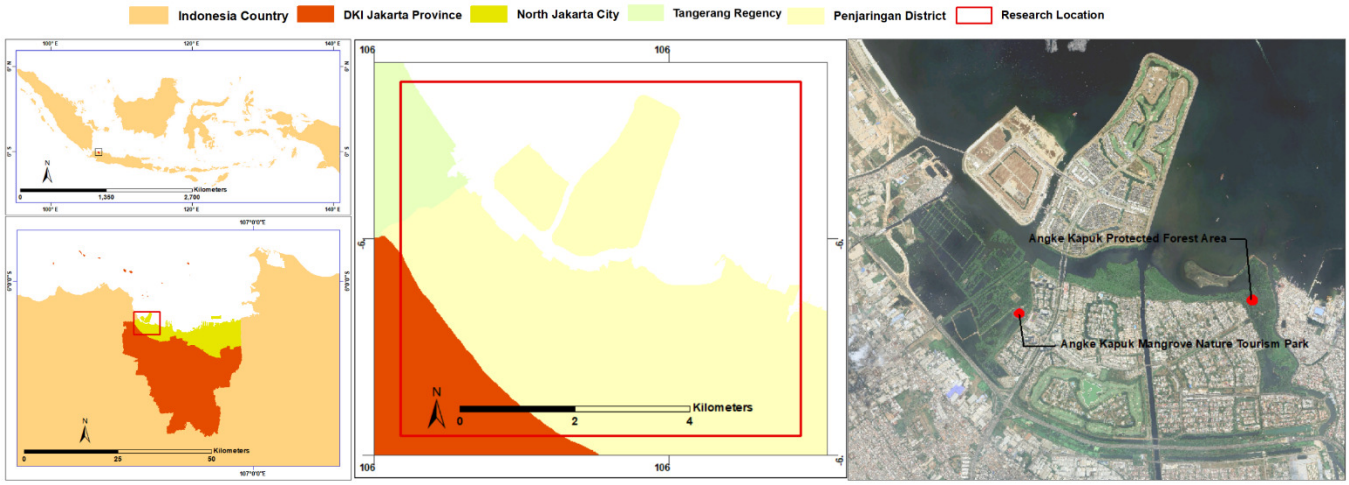

Fig. 2. Location of the MAK mangrove in Penjaringan, North Jakarta.

C. Satellite Imagery Pre-Processing

All scenes underwent geometric/radiometric correction and atmospheric correction to TOA/BOA reflectance [7]. For post-2003 Landsat-7 ETM+, multi-date SLC-off gap-filling was applied to reconstruct the approximately 22% missing data per scene (notably along image edges) and reduce bias [8]. Despite this, LST from ETM+ (2005‑2010) remains less accurate compared to Landsat-8 OLI/TIRS (≥2013), especially over highly heterogeneous areas; this gap-filling dependency is acknowledged as a study limitation.

D. Land Surface Temperature

LST—widely used for assessing drought, LULC change, land degradation, urban heat, and broader climate signals—was derived from Landsat-7 ETM+ Band 6 (2005, 2010; 60 m resampled to 30 m) and Landsat-8 TIRS Band 10 (2015, 2020, 2024; 100 m resampled to 30 m) [9, 10]. Radiance was converted to brightness temperature and corrected for land-surface emissivity via an NDVI-based method (°C). The uncertainty in LSE (often NDVI-derived) and coarse native TIR resolution can introduce mixed-pixel effects and bias in heterogeneous urban mosaics [11, 12]. Processing in ArcGIS/QGIS produced spatiotemporal LST maps for the MAK mangroves across pre- and post-reclamation periods.

E. Land Cover Classification

Land cover was mapped at five epochs (2005, 2010, 2015, 2020, 2024) using OBIA on Google Earth Pro mosaics (approximately 2 m) in eCognition, integrating spectral–spatial features for segmentation and class assignment [13, 14] (workflow in Figure 3). While GE imagery offers broad coverage, fine detail, and free access, its multi-sensor mosaic and limited metadata reduce spectral consistency and complicate multitemporal/radiometric analyses; thus, it is best suited to visualization and manual interpretation [3, 15]. For quantitative, larger-scale analyses, Sentinel-2 (10–20 m, approximately 5-day revisit, full metadata) provides higher inter-temporal spectral consistency.

The workflow for OBIA land-cover classification is illustrated in Figure 3.

F. Classification Accuracy Assessment

OBIA maps were validated against independent Google Earth Pro (approximately 2 m resolution) reference points using stratified random sampling per class and year (50 points/class; 300 total per epoch, 2005–2024). The Overall Accuracy (OA), Cohen's k, and class-wise F1 were computed,

as presented in Table II. The results yielded OA = 83.06–93.69% and k = 0.76–0.91.

G. Regression Analysis

The association between LST and land-cover composition was modeled via multiple linear regression [16], with predictors such as the areal fractions of the built-up area, mangrove, non-mangrove vegetation, open land, water, and ponds:

$$Y = a_0 + a_1.x_1 + a_2.x_2 + \ ... \ + a_n.x_n \quad (1)$$

where a_n and x_n are coefficients and land-cover variables, respectively. Estimation and basic diagnostics were performed in SPSS, and the coefficients were interpreted to quantify each land-cover class's marginal effect on LST.

H. Spatial Analysis Unit (150×150 m Grid)

A 150 m × 150 m grid was adopted because (i) Landsat-8's 30 m TIR permits 25 LST pixels per cell, stabilizing cell means and aligning with 5×5 smoothing windows [17], and (ii) the size is a multiple of the native resolution, aiding replication and LST-based spatial analysis. Empirical evidence also indicates that LST–urban morphology relations are stable at approximately 150 m, capturing local variability effectively [18].

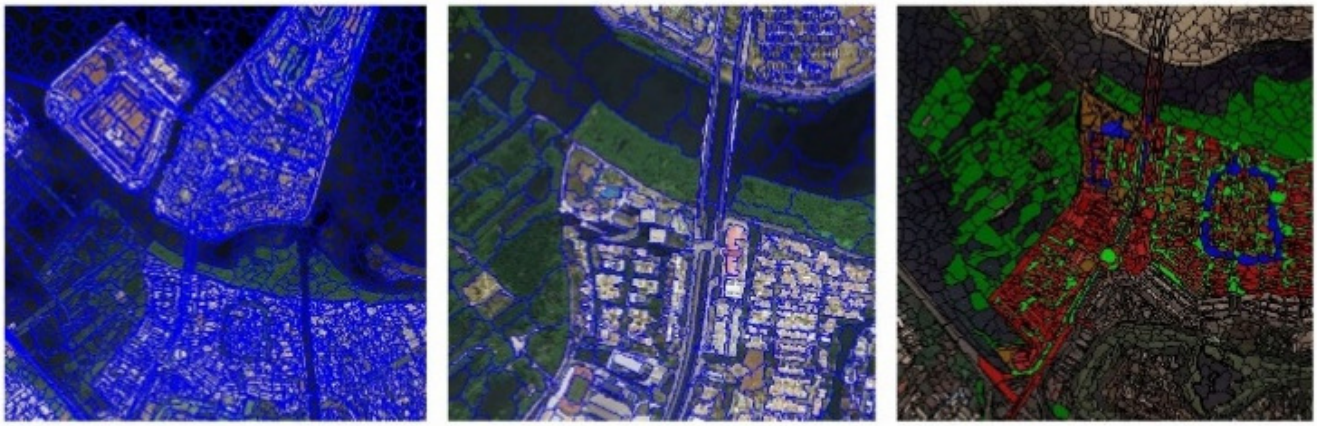

Fig. 3. OBIA workflow for land-cover classification.

TABLE I. SATELLITE DATA SOURCES

Platform	Bands	Variable	Native resolution (resampled)	Epochs
Landsat-7 ETM+	Band 6 (thermal)	LST	60 m to 30 m)	2005, 2010
Landsat 8 OLI/TIRS	Band 10; OLI	LST, NDVI	100 m to 30 m; 30 m	2015, 2020, 2024
Google Earth Pro	RGB mosaic	Land cover (OBIA)	≈2 m	2005–2024 (selected years)

TABLE II. RESULTS OF LAND COVER CLASSIFICATION ACCURACY TESTS

Year	2005	2010	2015	2020	2024
OA	83.06%	90.46%	87.67%	88.00%	93.69%
Cohen's k	0.762394	0.865753	0.836733	0.835831	0.91265
	Per-class *F1*				
Built-up land	0.6977	0.9048	0.8862	0.8478	0.9565
Mangrove	0.9286	0.9677	0.8485	0.8571	0.9674
Water	0.9318	0.9395	0.9479	0.9264	0.9345
Pond	0.5817	0.7797	0.8571	0.8800	0.9285
Open land	0.7090	0.5600	0.7692	0.6977	0.7333
Non-mangrove vegetation	0.9083	0.9535	0.8070	0.9459	0.9275

III. RESULTS AND DISCUSSION

A. Land-Cover Dynamics (2005–2024)

The high-resolution OBIA classification from Google Earth Pro produced reliable land-cover maps for MAK and enabled temporal comparison across 2005, 2010, 2015, 2020, and 2024 [19, 20]. The built-up area increased from 716.1 ha (2005) to 1,525.1 ha (2024), while mangroves expanded and water bodies/ponds declined. The open land peaked in 2015 and then decreased thereafter, with non-mangrove vegetation fluctuating moderately, as displayed in Figure 4 and Table III.

B. LST Trends

Landsat-derived LST shows sustained warming: mean LST increased from 20.2 °C in 2005 to 27.7 °C in 2024, with minima–maxima up to 23.6–36.0 °C. The sharpest rise occurred in 2010–2015, coincident with intensive land conversion and consistent with the heat amplification from impervious cover [21], as portrayed in Figure 5 and Table IV.

C. Thermal Behavior by Class

By land-cover class, the built-up areas consistently record the highest mean LST, followed by open land, whereas water bodies and mangroves are the coolest—reflecting the thermal behavior of impervious materials and the cooling effects of green–blue infrastructure [22, 23]. Mangroves additionally contribute to climate regulation via carbon sequestration, reinforcing their value as cooling "hot-spots" [24, 25], as depicted in Figure 6. These patterns are consistent with other tropical systems, notably the Sundarbans (Bangladesh–India), where NDVI increases are negatively correlated with LST [26]. Dense vegetation (e.g., mangroves) cools surface temperatures, yet cover transitions, degradation, and ecological stress can dampen this effect. Despite the cooling role of vegetation, year-to-year warming persists as land-use change and environmental variability co-drive thermal dynamics.

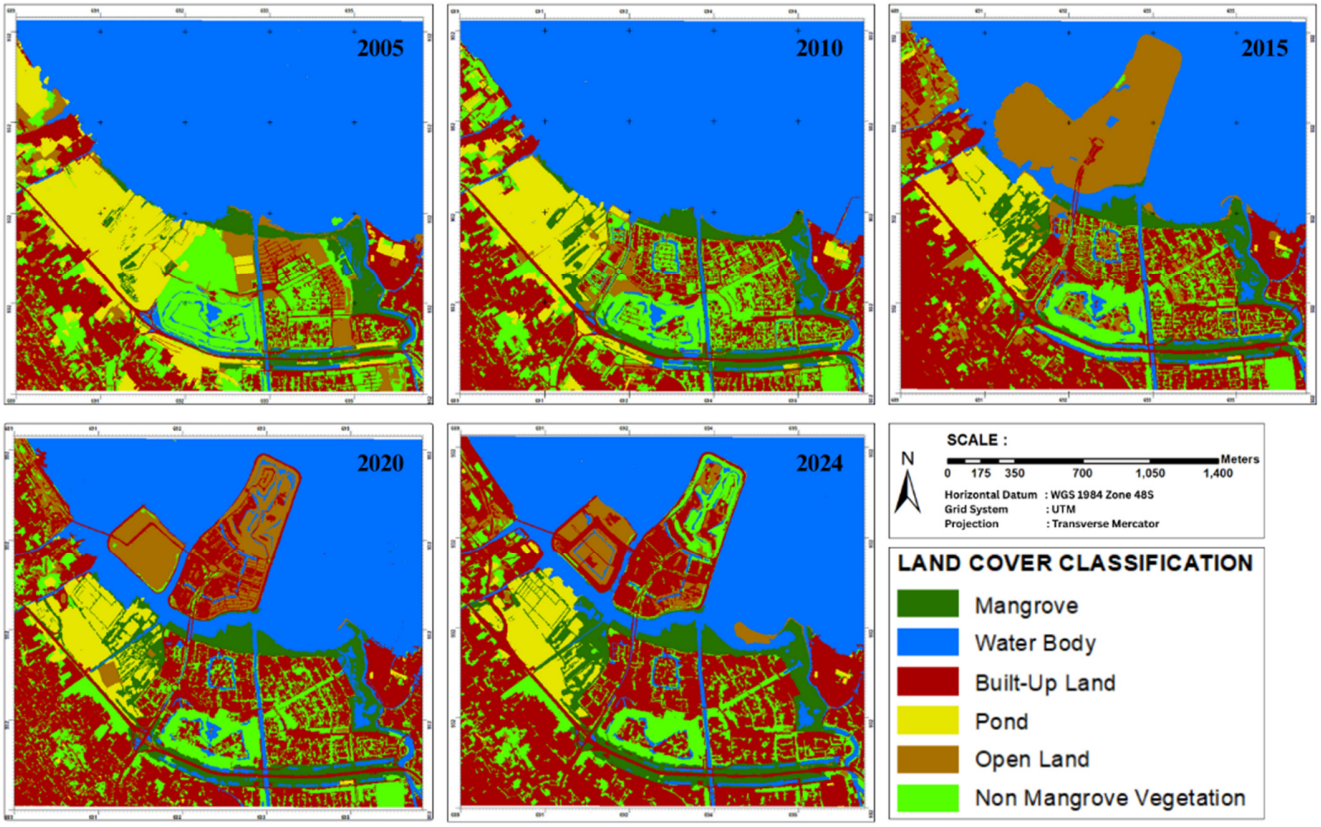

Fig. 4. Land cover changes from 2005 to 2024.

TABLE III. AREA OF LAND COVER TYPES IN 2005-2024 AT RESEARCH SITES

Land Cover	Area (ha)				
	2005	2010	2015	2020	2024
Built-up land	716.10	940.20	1,211.60	1,340.50	1,525.10
Mangrove	183.70	230.00	247.20	283.50	324.60
Water bodies	2,046.80	2,054.80	1,474.90	1,606.50	1,520.40
Pond	520.60	325.60	223.00	197.30	194.60
Open land	211.10	74.60	638.50	303.40	164.90
Non-mangrove vegetations	570.00	623.20	453.00	517.10	518.80

TABLE IV. LST STATISTICS (MIN-MAX-MEAN) FROM 2005 TO 2024

Years	LST value		
	LST min	LST max	LST mean
2005	17.10	27.00	20.20
2010	19.30	30.40	23.20
2015	21.80	30.40	24.90
2020	20.20	34.00	26.06
2024	23.60	36.00	27.70

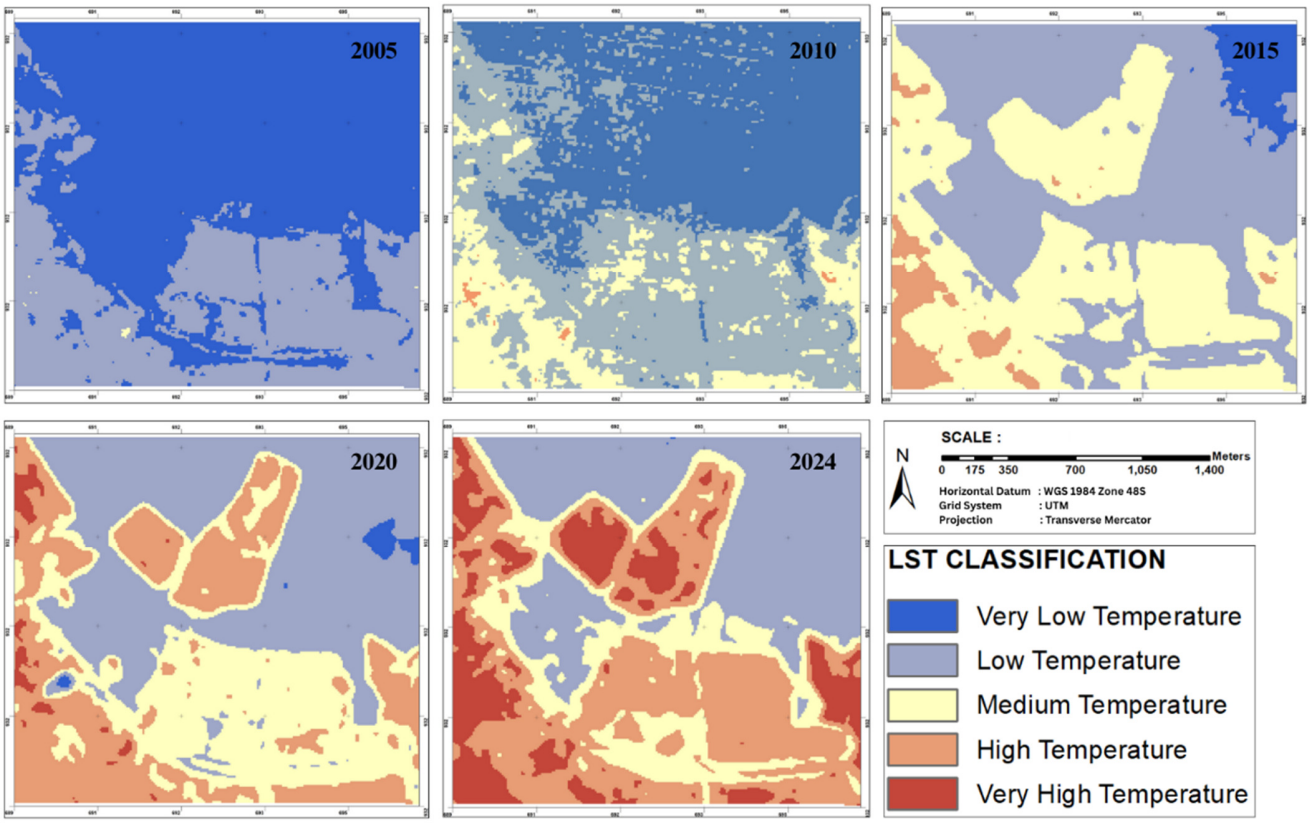

Fig. 5. LST changes from 2005 to 2024.

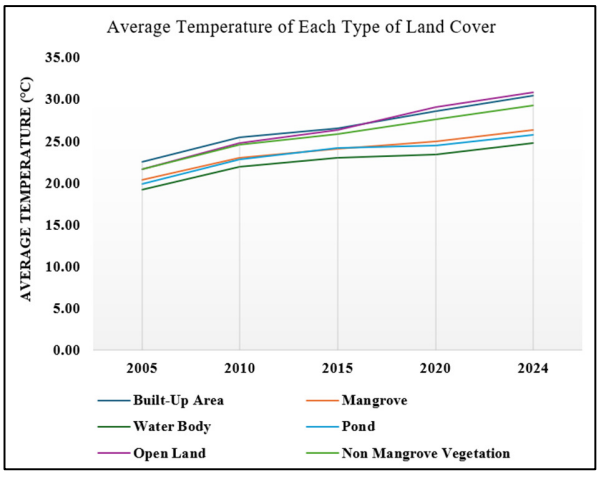

Fig. 6. Average temperature of each type of land cover.

D. Regression Evidence for Green–Blue Cooling

Multiple linear regressions, over 242 grids (150×150 m), show positive associations for the built-up area (B = 1.619) and open land (B = 1.139), and negative for mangroves (B = –0.960), water (B = –0.478), ponds (B = –0.275), and non-mangrove vegetation (B = –0.469). The model explains 95.1% of spatial LST variance (R^2 = 0.951, all $p < 0.001$, Variance Inflation Factor (*VIF*) = 1.153–2.613), confirming the cooling role of green–blue covers [27-29]. Table V presents the model summary and coefficients *B, SE, t, p,* and *VIF*.

The obtained regression model is:

$$Y_{LST} = 28.086 + 1.619(X_1) - 0.960(X_2) + 1.139(X_3) - 0.478(X_4) - 0.275(X_5) - 0.469(X_6))$$

where X_1 is the built-up land, X_2 is the mangrove area, X_3 is the open land, X_4 is the water body area, X_5 is the pond area, and X_6 is the non-mangrove vegetation. When this model is applied to the coastal fringe of Penjaringan (MAK), the results imply that integrating mangrove conservation/restoration and wider green–blue planning can moderate LST, aligning with evidence from Rotterdam in Netherlands [30], Gandhinagar in India [28], Malang in Indonesia [4, 14, 19, 31], and Jakarta's long-term urban warming context [6], while the wider ecosystem-service/blue-carbon co-benefits of mangroves strengthen coastal resilience [1, 2, 25], and relate to thermal comfort/public-health considerations in tropical cities [9].

E. Study Limitations

This study has the following limitations:

- A multi-temporal design using one Landsat scene per epoch (2005, 2010, 2015, 2020, and 2024), which captures long-term trends but may miss seasonal variability (monsoon cycles, soil moisture, cloud contamination); thus, the reported LST values are single-date snapshots rather than annual conditions. Future work should adopt multi-date sampling per year or higher-temporal products (e.g., MODIS, Sentinel-3).

- The absence of field ground truth means that validation relied on visual interpretation, increasing uncertainty in spectrally similar or heterogeneous areas.
- Image-based limitations can bias classification and LST estimation—atmospheric effects, mixed pixels, and the coarse native thermal resolution—potentially reducing precision. The findings should, therefore, be interpreted with appropriate caution.

TABLE V. REGRESSION TEST RESULTS FOR LST PREDICTION

	B	Standard errors	*t*-Values	*p*-Values	*VIF*
(Constant)	28.086	0.094	298.77	<0.001	-
Built-up land	1.619	0.069	23.46	<0.001	1.707
Mangrove	-0.960	0.059	-16.27	<0.001	1.810
Open land	1.139	0.095	11.99	<0.001	1.153
Water body	-0.478	0.069	-6.93	<0.001	2.130
Pond	-0.275	0.070	-3.93	<0.001	1.606
Non-mangrove vegetation	-0.469	0.072	-6.51	<0.001	2.613

IV. CONCLUSION

This two-decade assessment demonstrates that an Object-Based Image Analysis (OBIA) land-cover workflow combined with Landsat-derived Land Surface Temperature (LST) captures rapid coastal urbanization in Muara Angke–Kapuk (MAK), North Jakarta, and its thermal consequences. The study found that the built-up area expanded from 716.1 to 1,525.1 ha, while mangroves increased by 76.7% (183.7 ha-324.6 ha). Simultaneously, mean LST increased by 7.5 °C (20.2°C-27.7 °C). A multiple regression over 242 grids (150× 150 m) explained 95.1% of spatial LST variance (R^2 = 0.951), with warming associations for the built-up area (B = 1.619 °C), open land (B = 1.139 °C), and cooling associations for mangroves (B = −0.960 °C), water bodies (B = −0.478 °C), ponds (B = −0.275 °C), and non-mangrove vegetation (B = −0.469 °C).

These results support the case for integrating mangrove conservation/restoration and broader green–blue planning to help moderate land-surface temperature along Jakarta's coastal fringe. The study limitations include the reliance on the available land-cover classes and the chosen grid resolution. Future work should analyze seasonal dynamics, incorporate texture/morphological predictors, and apply spatial-block validation to strengthen generalization.

DATA AVAILABILITY STATEMENT

The Landsat imagery used in this study is publicly available from the United States Geological Survey (USGS) EarthExplorer portal at https://earthexplorer.usgs.gov/

ACKNOWLEDGMENT

The authors would like to thank all parties who have contributed to the completion of this research. This is an independent study and received no specific funding from any agency in the public, commercial, or not-for-profit sectors.

REFERENCES

[1] E. B. Barbier, S. D. Hacker, C. Kennedy, E. W. Koch, A. C. Stier, and B. R. Silliman, "The Value of Estuarine and Coastal Ecosystem Services," *Ecological Monographs*, vol. 81, no. 2, pp. 169–193, May 2011, https://doi.org/10.1890/10-1510.1.

[2] D. M. Alongi *et al.*, "Indonesia's Blue Carbon: A Globally Significant and Vulnerable Sink for Seagrass and Mangrove Carbon," *Wetlands Ecology and Management*, vol. 24, no. 1, pp. 3–13, Feb. 2016, https://doi.org/10.1007/s11273-015-9446-y.

[3] C. Giri, "Recent Advancement in Mangrove Forests Mapping and Monitoring of the World Using Earth Observation Satellite Data," *Remote Sensing*, vol. 13, no. 4, Feb. 2021, Art. no. 563, https://doi.org/10.3390/rs13040563.

[4] A. W. Hasyim, B. M. Sukojo, I. A. Anggraini, E. R. Fatahillah, and A. Isdianto, "Urban Heat Island Effect and Sustainable Planning: Analysis of Land Surface Temperature and Vegetation in Malang City," *International Journal of Sustainable Development and Planning*, vol. 20, no. 2, pp. 683–697, Feb. 2025, https://doi.org/10.18280/ijsdp.200218.

[5] M. Mas'uddin, L. Karlinasari, S. Pertiwi, and E. Erizal, "Urban Heat Island Index Change Detection Based on Land Surface Temperature, Normalized Difference Vegetation Index, and Normalized Difference Built-Up Index: A Case Study," *Journal of Ecological Engineering*, vol. 24, no. 11, pp. 91–107, Nov. 2023, https://doi.org/10.12911/22998993/171371.

[6] S. Siswanto, *et al.*, "Temperature, Extreme Precipitation, and Diurnal Rainfall Changes in the Urbanized Jakarta City During the Past 130 Years," *International Journal of Climatology*, vol. 36, no. 9, pp. 3207–3225, July 2016, https://doi.org/10.1002/joc.4548.

[7] J. R. Yepez Ramírez, R. R. Ricaurte Parraga, and J. A. Verdugo Arcos, "Use of Geomatic Techniques for Mapping Suspended Solids in Aquatic Ecosystems: The Case Study of Guayas River, Ecuador," *Engineering, Technology & Applied Science Research*, vol. 14, no. 6, pp. 17650–17656, Dec. 2024, https://doi.org/10.48084/etasr.8664.

[8] Y. Li, Q. Liu, S. Chen, and X. Zhang, "An Improved Gap-Filling Method for Reconstructing Dense Time-Series Images from LANDSAT 7 SLC-Off Data," *Remote Sensing*, vol. 16, no. 12, June 2024, Art. no. 2064, https://doi.org/10.3390/rs16122064.

[9] S. Patel, M. Indraganti, and R. N. Jawarneh, "A Comprehensive Systematic Review: Impact of Land Use/ Land Cover (LULC) on Land Surface Temperatures (LST) and Outdoor Thermal Comfort," *Building and Environment*, vol. 249, Feb. 2024, Art. no. 111130, https://doi.org/10.1016/j.buildenv.2023.111130.

[10] F. Mirchooli, S. H. Sadeghi, and A. Khaledi Darvishan, "Analyzing Spatial Variations of Relationships between Land Surface Temperature and Some Remotely Sensed Indices in Different Land Uses," *Remote Sensing Applications: Society and Environment*, vol. 19, Aug. 2020, Art. no. 100359, https://doi.org/10.1016/j.rsase.2020.100359.

[11] Z.-L. Li *et al.*, "Satellite-Derived Land Surface Temperature: Current Status and Perspectives," *Remote Sensing of Environment*, vol. 131, pp. 14–37, Apr. 2013, https://doi.org/10.1016/j.rse.2012.12.008.

[12] J. C. Jimenez-Munoz and J. A. Sobrino, "A Single-Channel Algorithm for Land-Surface Temperature Retrieval from ASTER Data," *IEEE Geoscience and Remote Sensing Letters*, vol. 7, no. 1, pp. 176–179, Jan. 2010, https://doi.org/10.1109/LGRS.2009.2029534.

[13] V. Kumar *et al.*, "GIS-Based Analysis of a Rainwater Harvesting System in the Multipurpose Hall of Quaid-e-Awam University of Engineering,

Science, and Technology," *Engineering, Technology & Applied Science Research*, vol. 12, no. 4, pp. 8837–8842, Aug. 2022, https://doi.org/10.48084/etasr.4995.

[14] A. W. Hasyim, I. A. Anggraini, F. Usman, and A. Isdianto, "Evaluating Urban Heat Island Effects in Malang City Parks Using UAV and OBIA Technologies," *International Journal of Sustainable Development and Planning*, vol. 20, no. 04, pp. 1633–1644, Apr. 2025, https://doi.org/10.18280/ijsdp.200425.

[15] M. Chi *et al.*, "Big Data for Remote Sensing: Challenges and Opportunities," *Proceedings of the IEEE*, vol. 104, no. 11, pp. 2207–2219, Nov. 2016, https://doi.org/10.1109/JPROC.2016.2598228.

[16] D. X. Tran *et al.*, "Characterizing the Relationship between Land use Land Cover Change and Land Surface Temperature," *ISPRS Journal of Photogrammetry and Remote Sensing*, vol. 124, pp. 119–132, Feb. 2017, https://doi.org/10.1016/j.isprsjprs.2017.01.001.

[17] D. Danniswari, T. Honjo, and K. Furuya, "Analysis of Building Height Impact on Land Surface Temperature by Digital Building Height Model Obtained from AW3D30 and SRTM," *Geographies*, vol. 2, no. 4, pp. 563–576, Sept. 2022, https://doi.org/10.3390/geographies2040034.

[18] A. Zhang and C. Xia, "Scale Effect on the Relationship between Urban Landscape Patterns and Land Surface Temperature," *Sustainable Cities and Society*, vol. 117, Dec. 2024, Art. no. 105942, https://doi.org/10.1016/j.scs.2024.105942.

[19] A. W. Hasyim*et al.*, "Assessing the Impact of Population Density and Land Use on Land Surface Temperature for Sustainable Urban Planning in Malang City, Indonesia," *International Journal of Sustainable Development and Planning*, vol. 20, no. 5, pp. 1679–2197, May 2025, https://doi.org/10.18280/ijsdp.200533.

[20] H. Gu, H. Li, L. Yan, Z. Liu, T. Blaschke, and U. Soergel, "An Object-Based Semantic Classification Method for High Resolution Remote Sensing Imagery Using Ontology," *Remote Sensing*, vol. 9, no. 4, Mar. 2017, Art. no. 329, https://doi.org/10.3390/rs9040329.

[21] H. Cai and X. Xu, "Impacts of Built-up Area Expansion in 2D and 3D on Regional Surface Temperature," *Sustainability*, vol. 9, no. 10, Oct. 2017, Art. no. 1862, https://doi.org/10.3390/su9101862.

[22] D. Kumar and S. Shekhar, "Statistical Analysis of Land Surface Temperature–Vegetation Indexes Relationship Through Thermal Remote Sensing," *Ecotoxicology and Environmental Safety*, vol. 121, pp. 39–44, Nov. 2015, https://doi.org/10.1016/j.ecoenv.2015.07.004.

[23] O. E. Adeyeri, A. A. Akinsanola, and K. A. Ishola, "Investigating Surface Urban Heat Island Characteristics Over Abuja, Nigeria: Relationship Between Land Surface Temperature and Multiple Vegetation Indices," *Remote Sensing Applications: Society and Environment*, vol. 7, pp. 57–68, Aug. 2017, https://doi.org/10.1016/j.rsase.2017.06.005.

[24] Y.-J. Shiau and C.-Y. Chiu, "Biogeochemical Processes of C and N in the Soil of Mangrove Forest Ecosystems," *Forests*, vol. 11, no. 5, Apr. 2020, Art. no. 492, https://doi.org/10.3390/f11050492.

[25] E. Sumarga, A. Sholihah, F. A. E. Srigati, S. Nabila, P. R. Azzahra, and N. P. Rabbani, "Quantification of Ecosystem Services from Urban Mangrove Forest: A Case Study in Angke Kapuk Jakarta," *Forests*, vol. 14, no. 9, Sept. 2023, Art. no. 1796, https://doi.org/10.3390/f14091796.

[26] K. Kanjin and B. M. Alam, "Assessing Changes in Land Cover, NDVI, and LST in the Sundarbans Mangrove Forest in Bangladesh and India: A GIS and remote sensing approach," *Remote Sensing Applications: Society and Environment*, vol. 36, Nov. 2024, Art. no. 101289, https://doi.org/10.1016/j.rsase.2024.101289.

[27] R. F. P. Murillo, W. Lavado Casimiro, Y. C. Pachac Huerta, M. Zapana Quispe, and D. Guevara-Freire, "Use of the SWAT Model to Simulate the Hydrological Response to LULC in a Binational Basin between Ecuador and Peru," *Engineering, Technology & Applied Science Research*, vol. 14, no. 6, pp. 17816–17823, Dec. 2024, https://doi.org/10.48084/etasr.8646.

[28] T. Modi *et al.*, "Geospatial Evaluation of Normalized Difference Vegetation Index (NDVI) and Urban Heat Island: A Spatio-temporal Study of Gandhinagar City, Gujarat, India," *Geomatics, Natural Hazards and Risk*, vol. 15, no. 1, Dec. 2024, Art. no. 2356214, https://doi.org/10.1080/19475705.2024.2356214.

[29] A. Isdianto, A. W. Hasyim, B. M. Sukojo, I. Alimuddin, I. A. Anggraini, and E. R. Fatahillah, "Integrating Urban Design with Natural Dynamics: Enhancing Ecological Resilience in Malang City over a Decade," *International Journal of Sustainable Development and Planning*, vol. 20, no. 3, pp. 1061–1075, Mar. 2025, https://doi.org/10.18280/ijsdp.200313.

[30] B. G. Heusinkveld, G. J. Steeneveld, L. W. A. Van Hove, C. M. J. Jacobs, and A. A. M. Holtslag, "Spatial Variability of the Rotterdam Urban Heat Island as Influenced by Urban Land Use," *Journal of Geophysical Research: Atmospheres*, vol. 119, no. 2, pp. 677–692, Jan. 2014, https://doi.org/10.1002/2012JD019399.

[31] T. Kusumadewi *et al.*, "Synthesizing Environmental, Social, and Urban Density Metrics to Predict Urban Heat Island Dynamics using Remote Sensing and Support Vector Regression," *Engineering, Technology & Applied Science Research*, vol. 15, no. 3, pp. 23141–23148, June 2025, https://doi.org/10.48084/etasr.9791.